Rheological Properties of Polypropylenes with Different Molecular Weight Distribution Characteristics

MITSUYOSHI FUJIYAMA, YOSHIYUKI KITAJIMA, HITOSHI INATA

Tokuyama Research Laboratory, Tokuyama Corp., 1-1, Harumi-cho, Tokuyama-shi, Yamaguchi-ken, 745-0024 Japan

Received 19 March 2001; accepted 10 July 2001

ABSTRACT: Relationships between the rheological properties and the molecular weight distribution of two polypropylene series with different molecular weight distribution characteristics were studied. The end correction coefficient in capillary flow is determined by the molecular weight M_w and the molecular weight distribution M_w/M_n, and is higher as both characteristic values are larger. The die swell ratio at a constant shear rate depends on M_w, M_w/M_n, and M_z/M_w, and is higher as the three characteristic values are larger. The critical shear rate at which a melt fracture begins to occurs depends on the molecular weight M_w and the molecular weight distribution M_z/M_w, and is proportional to M_z/M_w^2 in a log–log plot. The critical shear stress does not depend on the molecular weight, and is higher as M_z/M_w is higher. The zero-shear viscosity is determined by a molecular weight of slightly higher order than M_w, and the characteristic relaxation time is determined by M_z. The storage modulus at a constant loss modulus scarcely depends on the molecular weight, and is higher as the molecular weight distribution M_w/M_n is higher. © 2002 Wiley Periodicals, Inc. J Appl Polym Sci 84: 2128–2141, 2002

Key words: poly(propylene); catalyst; molecular weight distribution; melt; rheology

INTRODUCTION

The Ziegler-Natta catalyst for polyolefins has been actively studied from both scientific and industrial aspects for about 45 years since its discovery. This made progress in the manufacturing processes and qualities of polyethylene and polypropylene (PP).

Particularly for the PP catalyst, the early $TiCl_3$-type catalyst has been improved to the $MgCl_2$-supported titanium catalyst, which has largely improved the activity of polymerization and the tacticity of polymer. As a result, the PP manufacturing process has been simplified from the deashing and washing process to the nondeashing and nonwashing process, and further to the ultimate gas-phase process. At the same time, the quality of the polymer also has made an improved step, leading to industrial production of PPs with high tacticity and crystallinity.

We study the effects of molecular structures (molecular weight distribution and tacticity) on qualities such as processing and product properties of PPs prepared by use of the $TiCl_3$-type catalyst and the $MgCl_2$-supported titanium catalyst. In the present article, rheological properties intimately related with the processing properties are studied. First, the molecular weight distribution characteristics of both series of PPs are investigated, then how they affect the rheological properties is studied, and last, the effect of molecular weight distribution on the rheological properties, and in turn, on the processing properties is clar-

Correspondence to: M. Fujiyama (m-fujiyama@tokuyama.co.jp).

Journal of Applied Polymer Science, Vol. 84, 2128–2141 (2002)

Table I Characteristics of Samples

Catalyst	Sample Name	MFI (g/10min)	Ethylene Content (wt %)	Isotactic Pentad Fraction	M_n (10^4)	M_w (10^4)	M_z (10^4)	M_{z+1} (10^4)	M_w/M_n	M_z/M_w	M_{z+1}/M_z
A	A-1	0.51	0.31		8.37	57.2	255	609	6.8	4.5	2.4
	A-2	1.77	0.33	0.951	8.26	40.0	158	460	4.8	4.0	2.9
	A-3	2.0	0	0.956	7.86	40.9	167	385	5.2	4.1	2.3
	A-4	4.0	0.35		5.77	31.6	123	259	5.5	3.9	2.1
	A-5	14.5	0		4.29	22.7	92	227	5.3	4.1	2.5
	A-6	32.6	0		2.76	16.6	70	169	6.0	4.2	2.4
B	B-1	0.49	0		8.02	63.0	212	395	7.9	3.4	1.9
	B-2	1.73	0	0.930	4.61	43.2	169	330	9.4	3.9	2.0
	B-3	4.0	0		3.53	32.1	147	289	9.1	4.6	2.0
	B-4	8.9	0		2.80	26.6	132	275	9.5	5.0	2.1
	B-5	14.7	0		2.67	23.8	127	264	8.9	5.3	2.1
	B-6	25.1	0		2.39	20.2	114	258	8.5	5.6	2.3

ified. The rheological properties studied are capillary flow properties such as flow curve, end correction, die swell, and melt fracture behaviors, and dynamic viscoelasticities such as complex viscosity, zero-shear viscosity, characteristic relaxation time, storage modulus, and loss modulus.

As for the product properties, the difference in structure and properties of injection moldings molded from both series of PPs is studied, and the effects of molecular weight distribution and tacticity on the structure and properties of the moldings are clarified in the following article.

EXPERIMENTAL

Samples

PPs prepared by the $MgCl_2$-supported titanium catalyst and by the $TiCl_3$-type catalyst are called cat.-A PPs and cat.-B PPs, respectively. The cat.-A PPs were prepared by use of a $MgCl_2$-supported $TiCl_4$ compound, which is generally used industrially, as a main catalyst, of $AlEt_3$ as a cocatalyst, and of an organic silane compound as a tacticity modifier (external donner). The polymerization was carried out in a medium of propylene monomer at 60–70°C. The MFI (molecular weight) was adjusted by use of hydrogen as the chain transfer. cat.-B PPs were prepared by use of a general δ-type $TiCl_3$ compound (Solvay-type catalyst) as a main catalyst, of $AlEt_2Cl$ as a cocatalyst, and of an organic ester compound as a tacticity modifier (external donner). The polymerization method is the same as that of cat.-A PPs.

Table I shows the characteristics of the samples. MFI (melt flow index) was measured at 230°C under a load of 2160 g according to ASTM D1238-62T. Ethylene content was measured by infrared spectroscopy. The isotactic pentad fraction was measured by ^{13}C-NMR. A-1 and B-1, A-2 and B-2, A-4 and B-3, and A-5 and B-5 have similar MFIs, respectively.

Measurements

Molecular Weight Distribution

Molecular weight distribution was measured with a gel permeation chromatography apparatus GPC150-C Type (Waters Ltd., USA) by use of a column system of 10^3, 10^4, 10^5, 10^6, and 10^7 Å and of *o*-dichlorobenzene as solvent.

Capillary Flow Properties

The relation between pressure P (Pa) and volumetric flow rate Q (cm^3/s) was measured at 230°C, with a capillary rheometer, Koka Flow Tester (Shimazu Seisakusho Co., Ltd., Japan) using straight dies of a diameter 2R = 0.5 mm, lengths L = 1, 2.5, and 5 mm, and L/R = 4, 10, and 20.

The apparent shear stress τ' and the apparent shear rate $\dot{\gamma}'$ at the wall in capillary flow are given by eqs. (1) and (2), respectively:

$$\tau' = \frac{PR}{2L} \tag{1}$$

$$\dot{\gamma}' = \frac{4Q}{\pi R^3} \tag{2}$$

The effective shear stress τ corrected by the entrance pressure loss P_0 at the capillary inlet, the true shear rate $\dot{\gamma}$ corrected by non-Newtonianity, and the true viscosity η are given by eqs. (3)[1], (4),[2] and (5), respectively:

$$\tau = \frac{(P - P_0)R}{2L} = \frac{R}{2(L + \nu R)} \quad (3)$$

$$\dot{\gamma} = \frac{1}{4}\left(3 + \frac{d\log\dot{\gamma}'}{d\log\tau}\right)\dot{\gamma}' \quad (4)$$

$$\eta = \frac{\tau}{\dot{\gamma}} \quad (5)$$

here, ν is the end correction coefficient corresponding to P_0.

Arranging eq. (3),

$$P = 2\tau\left(\frac{L}{R}\right) + 2\nu\tau \quad (6)$$

a straight line should be obtained if pressure P required to produce a definite shear stress τ and, hence, a definite shear rate $\dot{\gamma}'$ is plotted against L/R (Bagley plot[1]), and the end correction coefficient ν is obtained as an intercept of L/R axis. By use of ν, the effective shear stress τ is obtained by eq. (3). Next, the apparent shear rate $\dot{\gamma}'$ is corrected to the true shear rate $\dot{\gamma}$ by eq. (4). In this way, the true flow curve ($\tau - \dot{\gamma}$ or $\eta - \dot{\gamma}$) is obtained.

After the extrudate solidified, its diameter D at the part 5 mm from the front was measured with a micrometer and the ratio D/D_0, where D_0 is the capillary diameter was called die swell ratio and used as a measure of die swell.

The appearance of the extrudate was observed with the naked eye, and the occurrence of melt fracture was checked.

Dynamic Viscoelasticity

The storage modulus $G'(\omega)$, loss modulus $G''(\omega)$, and absolute value of complex viscosity $|\eta^*|(\omega)$ were measured at 170, 200, and 240°C under N_2 atmosphere with a concentric cylinder rheometer, Rheometer Almighty (Iwamoto Seisakusho Co., Ltd., Japan). The zero-shear viscosity η_0 was obtained as the value of $|\eta^*|(\omega)$ at low ω. The characteristic relaxation time λ_0 was obtained from ω_0 where $|\eta^*|(\omega)$ drops to 0.8 η_0 according to the Graessley's empirical formula:[3]

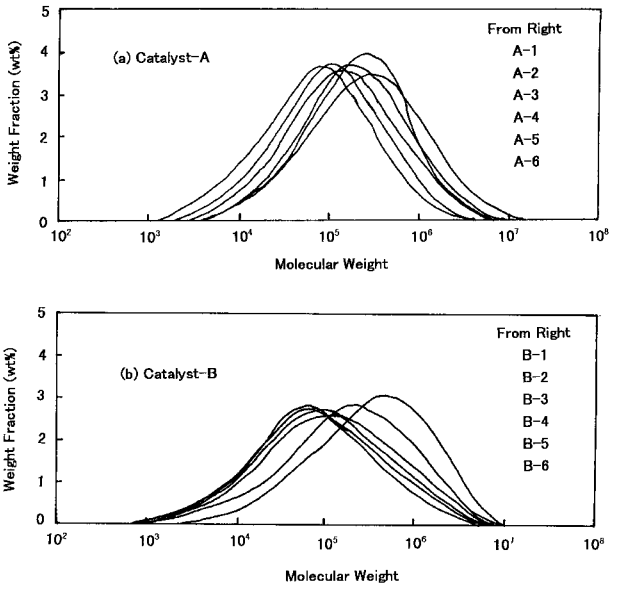

Figure 1 Molecular weight distribution curves of (a) cat.-A PPs and (b) cat.-B PPs.

$$\omega_0\lambda_0 = 0.6 \quad (7)$$

RESULTS AND DISCUSSION

Molecular Weight Distribution

Figure 1(a) and (b) shows the molecular weight distribution curves of cat.-A PPs and cat.-B PPs, respectively, and various average molecular weights are shown in Table I. It is seen in Figure 1 that the shape of molecular weight distribution curve of cat.-A PPs scarcely depends on MFI, and the curve shifts in parallel to the molecular weight axis according to MFI. As for cat.-B PPs, the shape of the curve at low molecular weight side from the peak scarcely changes by MFI, whereas the high molecular weight side from the peak narrows with decreasing MFI.

Figure 2 shows the changes of various average molecular weights with MFI. Compared at the same MFI, M_n is higher for cat.-A PPs, M_w shows little difference between both series PPs , and M_z and M_{z+1} are higher for cat.-A PPs at low MFI, reversing at high MFI. The slope of dependence of each average molecular weight on MFI is nearly the same for cat.-A PPs, whereas it decreases with increasing the order of average for cat.-B PPs.

Figure 3 shows the changes of various molecular weight distribution parameters, M_w/M_n, $M_z/$

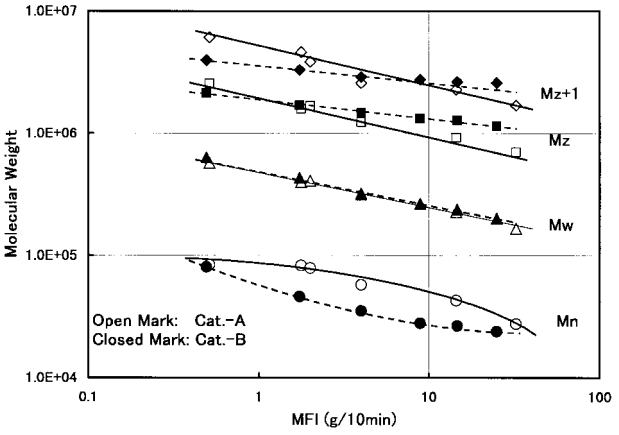

Figure 2 Changes of various average molecular weights with melt flow index (MFI).

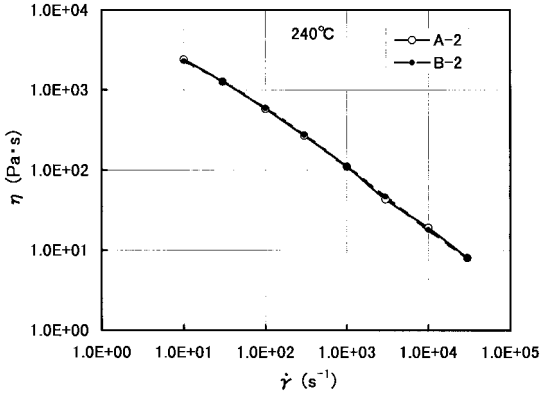

Figure 4 Flow curves (viscosity η–shear rate $\dot{\gamma}$) of A-2 and B-2 samples at 240°C.

M_w, and M_{z+1}/M_z with MFI. Although M_w/M_n shows large scattering, it scarcely depends on MFI for both series of PPs and their values are 5.5 and 9 for cat.-A PPs and cat.-B PPs, respectively, the former being lower than the latter. M_z/M_w, a parameter of molecular weight distribution at high molecular weight region, increases with increasing MFI for cat.-B PPs, whereas it scarcely depends on MFI for cat.-A PPs. As a result, cat.-A PPs show higher M_z/M_w than cat.-B PPs at low MFI; the order reverses at an MFI of about 2 g/10 min, and cat.-B PPs show higher M_z/M_w at high MFI. Frank[4] reports in an article of 1966 that a molecular weight distribution of PP measured rheologically narrows with increasing molecular weight. Mieras and Rijn[5] report in an article of 1969 that M_z/M_w of PP narrows with increasing M_w. These tendencies are similar to that of cat.-B PPs. cat.-B PPs were manufactured before 1989.

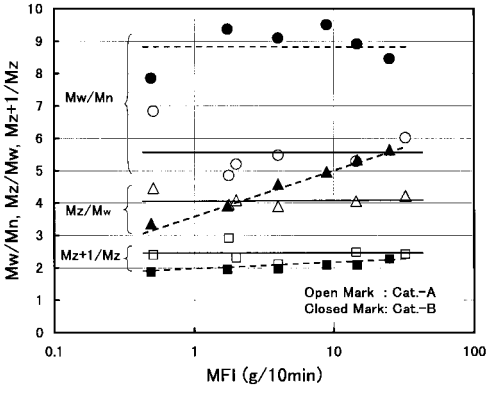

Figure 3 Changes of various molecular weight distribution parameters with melt flow index (MFI).

There is a possibility that the PPs used in these three studies are prepared by similar catalyst systems. M_{z+1}/M_z, a parameter of molecular weight distribution at a still higher molecular weight region, slightly increases with increasing MFI for cat.-B PPs, whereas it scarcely depends on MFI for cat.-A PPs. Furthermore, cat.-A PPs show slightly higher M_{z+1}/M_z than cat.-B PPs, reversing in the case of M_w/M_n.

Capillary Flow Properties

Flow Curve

The true viscosity η was calculated from the effective shear stress τ corrected in the end effect by eq. (3) and the true shear rate $\dot{\gamma}$ corrected in non-Newtonianity by eq. (4). As a result, no substantial significant difference in viscosity at $\dot{\gamma} = 10^1 - 3 \times 10^4$ s^{-1} was found between cat.-A PPs and cat.-B PPs. As an example, a comparison in flow curve between A-2 and B-2 samples that have similar MFIs is shown in Figure 4. They show a similar behavior, from which both series PPs are assumed to behave similarly in the shear rate range that a molten resin encounters at extrusion and injection molding.

End Correction

The change of the end correction coefficient ν with shear rate $\dot{\gamma}'$ of each sample at each temperature was obtained from Bagley plots according to eq. (6). Figure 5 shows its example for A-2 sample. ν increases with $\log\dot{\gamma}'$ in an upward tendency. In the following article, PPs used in the present study will be injection molded, and the structure and properties of the moldings will be studied.

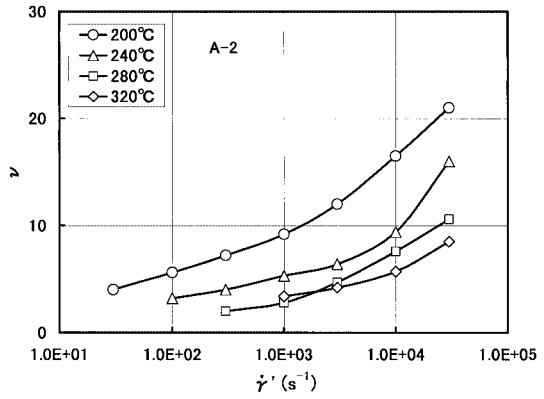

Figure 5 Change of end correction coefficient ν with apparent shear rate $\dot{\gamma}'$ for A-2 sample.

Because the shear rate that a molten resin encounters at the gate of the mold in the following study is 4200 s^{-1}, ν at $\dot{\gamma}' = 4200$ s^{-1} will be examined for the reference of the following study. As shown in Figure 5 as an example, because the shape of curve of ν vs. log$\dot{\gamma}'$ plot is similarly independent of sample and temperature and only its position shifts in parallel to log $\dot{\gamma}'$-axis according to the sample and temperature, ν at other $\dot{\gamma}'$ changes only in absolute value, and shows similar behaviors to that at 4200 s^{-1}. Figure 6(a) and (b) shows the changes of ν at $\dot{\gamma}' = 4200$ s^{-1} with temperature for cat.-A PPs and cat.-B PPs, respectively. ν decreases with temperature. ν continues to decrease even at high temperatures for cat.-A PPs. Although the slope of decrease in ν of cat.-B PPs is higher than that of cat.-A PPs below 280°C, it tends to level off or turn to increase at high temperatures. The fact that ν decreases with temperature is generally observed for PP[6,7] and other polymers.[8–17] As a large tendency, ν is higher as MFI is lower or the molecular weight is higher. This tendency is also generally reported for PP[7,18–21] and other polymers.[12,14,17,22–24] Compared at a similar MFI (molecular weight), cat.-B PPs with generally broader molecular weight distribution tend to show higher ν. The same tendency is reported for PP by Kamide and Fujii[7] and Fujiyama and Awaya,[19] for HDPE by LaMantia et al.[18] and for chloroprene by Kawasaki et al.[23,24] From the above, it may be said that ν of PP is higher as the temperature is lower, the shear rate is higher, the molecular weight M_w is higher, and the molecular weight distribution M_w/M_w is broader.

Die Swell

Figure 7(a) and (b) shows the changes, with shear rate, of the die swell ratio D/D_0 measured by use of a die of L/R = 20 at 240°C for cat.-A PPs and cat.-B PPs, respectively, as examples. Because D/D_0 measured by use of a die with smaller L/R at lower temperature shows a relatively higher value, it is enough to examine only the value measured by use of a die of L/R = 20 at 240°C when compared among samples. The die swell ratio increases with shear rate. Although the die swell ratio tends to show higher value as the MFI is lower or the molecular weight is higher for cat.-A PPs, it shows a nearly constant value independent of MFI for cat.-B PPs. The die swell ratio at a constant shear rate is generally higher as the molecular weight is higher and the molecular weight distribution is broader. The former (effect of molecular weight) is reported for PP,[25] PE,[26,27] HDPE,[28] and polychloroprene.[24,29] The latter (effect of molecular weight distribution) is reported for PP in relation to general molecular weight

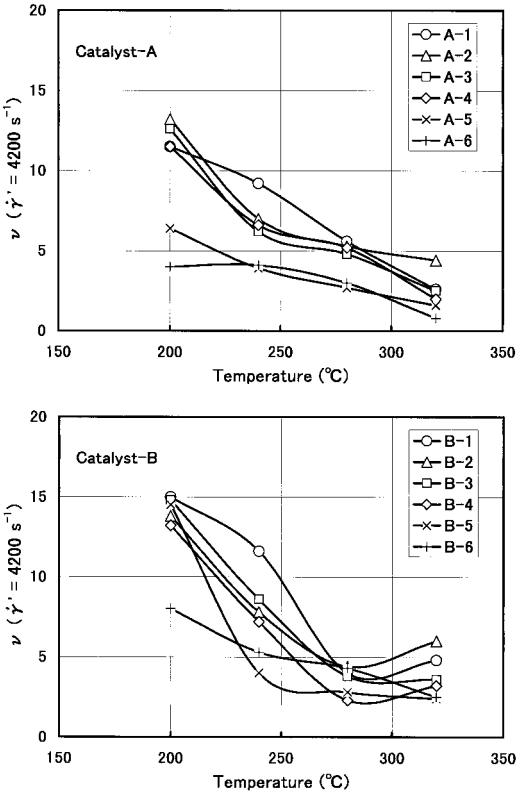

Figure 6 (a) Temperature change of end correction coefficient ν at $\dot{\gamma}' = 4200$ s^{-1} for cat.-A PPs. (b) Temperature change of end correction coefficient ν at $\dot{\gamma}' = 4200$ s^{-1} for cat.-B PPs.

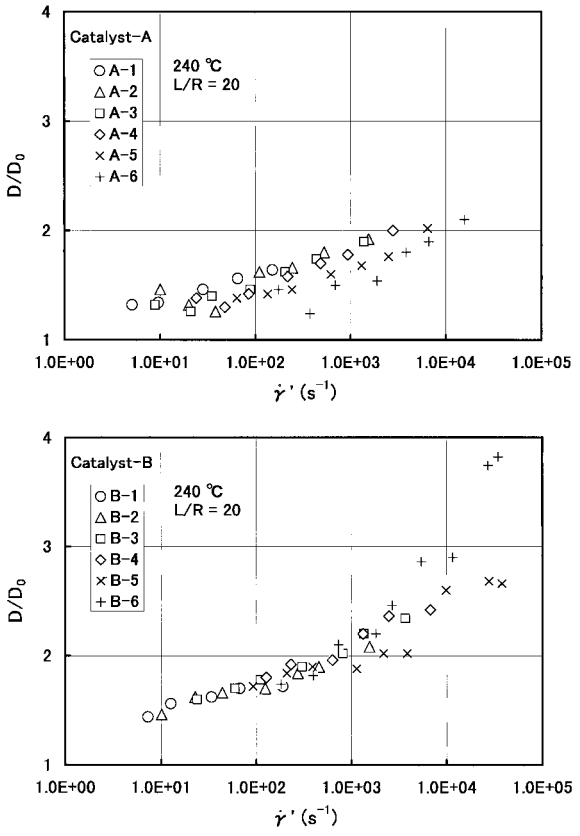

Figure 7 (a) Change of die swell ratio D/D_0 with shear rate $\dot{\gamma}'$ for cat.-A PPs at 240°C. (b) Change of die swell ratio D/D_0 with shear rate $\dot{\gamma}'$ for cat.-B PPs at 240°C.

distribution,[19] for PE in relation to M_w/M_n,[27] for HDPE in relation to M_w/M_n,[28] and for polychloroprene in relation to M_z/M_w.[24] The fact that the die swell ratio of cat.-A PPs is higher as the MFI is lower is assumed to be because the molecular weight distribution is independent of the MFI, and almost constant, as shown in Figures 1 and 3, and hence, the effect of only molecular weight must appear. The fact that the die swell ratio of cat.-B PPs is constant independent of MFI is assumed to be because M_z/M_w is higher for higher MFI resin, as shown in Figure 3, and hence, the increase of the die swell ratio due to an increase of molecular weight balances the decrease of die swell ratio due to a decrease of M_z/M_w, the die swell ratio being just constantly independent of MFI. Furthermore, the fact that cat.-B PPs generally show higher die swell ratios than cat.-A PPs is assumed to be because the former have higher M_w/M_ns than the latter, as shown in Figure 3. Summarizing the above experimental results, the die swell ratio of PP at constant shear rate is governed by the molecular weight M_w, and the molecular weight distributions M_w/M_n and M_z/M_w, and is higher as these three parameters are higher. As for the extrusion conditions, the die swell ratio becomes higher when extruded by use of a die of small L/R at high shear rate at low temperature.

Melt Fracture

Figure 8(a) and (b) shows the changes of the critical shear rates $\dot{\gamma}_c'$ at which a melt fracture begins to occurs with temperature for cat.-A PPs and cat.-B PPs, respectively. These $\dot{\gamma}_c'$s are averaged ones of the values obtained by use of dies of three L/Rs. $\dot{\gamma}_c'$ increases with temperature. Figure 9 shows the change of $\dot{\gamma}_c'$ at 200°C with MFI. cat.-A PPs show higher $\dot{\gamma}_c'$ than cat.-B PPs at low MFI; both series PPs show similar $\dot{\gamma}_c'$ at MFI $\fallingdotseq$ 2 g/10min, and cat.-B PPs inversely show higher $\dot{\gamma}_c'$ than cat.-A PPs at higher MFI. For cat.-B PPs, $\dot{\gamma}_c'$ of B-6 could not be measured due to too high a value. The change of $\dot{\gamma}_c'$ with MFI is similar to the

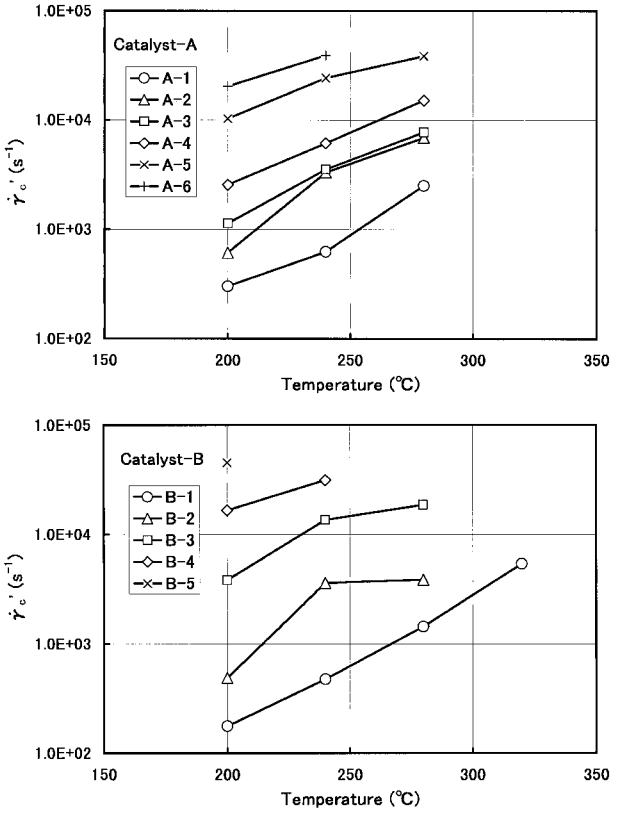

Figure 8 (a) Temperature change of critical shear rate $\dot{\gamma}_c'$ for cat.-A PPs. (b) Temperature change of critical shear rate $\dot{\gamma}_c'$ for cat.-B PPs.

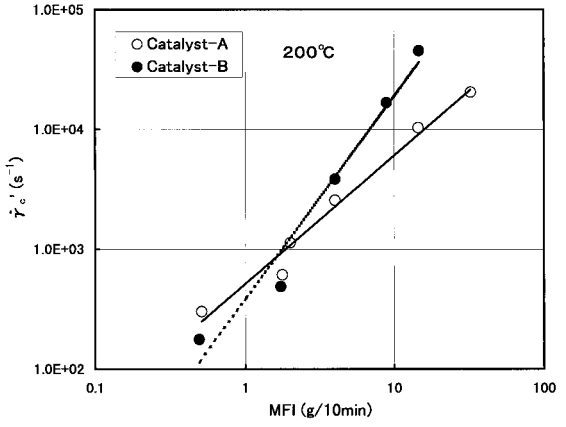

Figure 9 Change of critical shear rate $\dot{\gamma}_c'$ at 200°C with melt flow index (MFI).

change of M_z/M_w with MFI in Figure 3, meaning that $\dot{\gamma}_c'$ is governed by the high-order molecular weight distribution M_z/M_w as well as the molecular weight. Figure 10 shows plots of $\dot{\gamma}_c'$ against the product $M_z/M_w{}^2$ of the reciprocal of weight-average molecular weight, $1/M_w$, and molecular weight distribution parameter M_z/M_w. Both quantities show a linear relationship in log–log plot independent of the kind of catalyst. This means that $\dot{\gamma}_c'$ is higher as the molecular weight M_w is lower, and the molecular weight distribution M_z/M_w is broader. Generally the extrusion operation must be carried out at a shear rate below $\dot{\gamma}_c'$ because the melt fracture deteriorates the extrudate appearance. Referring to Figure 10, a high-speed extrusion is possible by extruding a resin with low molecular weight and broad molecular weight distribution at high temperature. The fact that $\dot{\gamma}_c'$ increases with temperature holds for any polymers and is common knowledge. The increase of $\dot{\gamma}_c'$ with increasing MFI or with decreasing molecular weight is also generally reported for PP[19,20] and other polymers.[9,17,23,29–34] As for the effect of molecular weight distribution, no study on PP is found. Stabler et al.[35] found that $\dot{\gamma}_c'$ of HDPE is higher as the molecular weight distribution is broader. Goyal et al.[36] report that $\dot{\gamma}_c'$ of LLDPE increases with increasing molecular weight distribution M_w/M_n below 10, and steeply drops at M_w/M_n above 10. The experimental fact in the present study that $\dot{\gamma}_c'$ of PP is determined by the molecular weight distribution M_z/M_w as well as the molecular weight M_w and increases with increasing $M_z/M_w{}^2$ is the first finding.

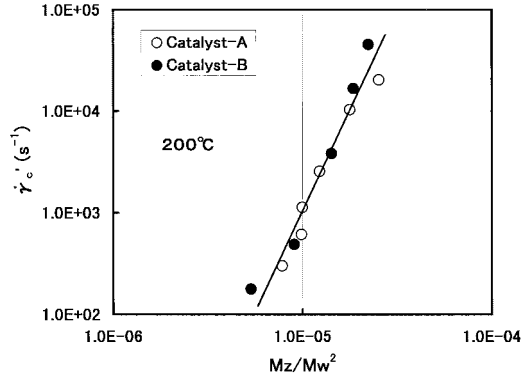

Figure 10 Relation between critical shear rate $\dot{\gamma}_c'$ at 200°C and $M_z/M_w{}^2$.

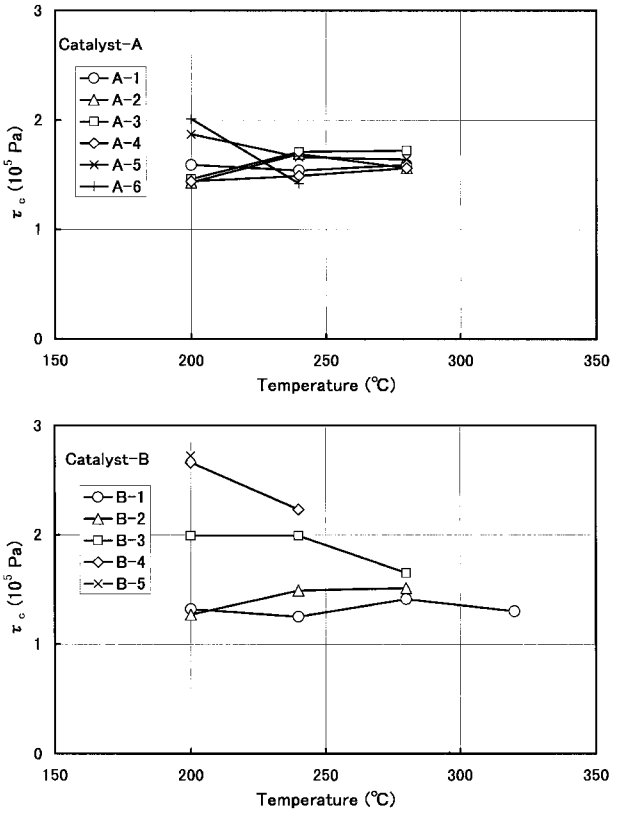

Figure 11 (a) Temperature change of critical shear stress τ_c for cat.-A PPs. (b) Temperature change of critical shear stress τ_c for cat.-B PPs.

Figure 11(a) and (b) shows the changes of the critical shear stress τ_c at which a melt fracture begins to occur with temperature for cat.-A PPs and cat.-B PPs, respectively. These τ_cs are averaged ones of the values obtained by use of dies of three L/Rs. τ_c is generally almost constant ($1 - 3 \times 10^5$ Pa) independent of temperature. While τ_c of cat.-A PPs is almost constant, independent of MFI or molecular weight, that of cat.-B PPs tends to

increase with increasing MFI or with decreasing molecular weight. τ_c values of 10^5–10^6 Pa are reported for many polymers.[37] As for the temperature dependence of τ_c, that τ_c scarcely changes or slightly increases with increasing temperature is reported for PP[38-41] and most other polymers,[11,17,38,39,42,43] and is main stream, a reverse tendency being reported for PVC.[15,34,44] As for the molecular weight dependence of τ_c, a reduction of τ_c with increasing molecular weight is reported for PP[19,29,41,45] and other polymers,[9,23,29–33,42,44] some reports[19,20,30] declaring $\tau_c \times M_w$ = constant ($3–4 \times 10^{10}$ Pa). Kamide et al.[25] report that τ_c of PP is constant, independent of the molecular weight. Sieglaff et al.[34] report that τ_c of PVC increases with the molecular weight. Vlachpoulos et al.[43] theoretically derived the dependence of τ_c on M_w according to the Graessley and Segal's theory,[46] and showed that generally $\tau_c \times M_w \propto M_w$ and as extreme cases $\tau_c \times M_w$ = constant when the entanglement density $E << 1$ and τ_c = constant when $E >> 1$. As for the dependence of τ_c on molecular weight distribution, the case[31] where τ_c increases with broadening the molecular weight distribution, the cases[33,42,43,47] where τ_c scarcely depends on the molecular weight distribution and the cases[35,41] where τ_c decreases with broadening the molecular weight distribution are variously reported, and there is no definite opinion. When studying the effect of molecular weight distribution, sometimes the molecular weight also changes, and hence, the study where the effect of only molecular weight distribution is extracted is scarcely found, which is assumed to be the cause of diversity of the experimental results. According to the present experimental results, τ_c is almost constant (about 1.5×10^5 Pa) independent of temperature and molecular weight for cat.-A PPs. On the other hand, τ_c scarcely depends on temperature, and tends to increase with increasing MFI or with decreasing molecular weight for cat.-B PPs. From the facts that the molecular weight distribution scarcely changes when the MFI or molecular weight changes for cat.-A PPs and that τ_c is constant independent of the molecular weight for cat.-A PPs, it may be said that the molecular weight scarcely affects τ_c. τ_c of cat.-B PPs is slightly lower than that of cat.-A PPs in the high molecular weight region, increases with decreasing molecular weight, and becomes higher than that of cat.-A PPs at the low molecular weight region.

Because it has been proven that τ_c of cat.-A PPs scarcely depends on the molecular weight, the fact that τ_c of cat.-B PPs increases with decreasing the molecular weight is due to the effect of molecular weight distribution M_z/M_w, and it may be said that τ_c increases with increasing M_z/M_w. Why the molecular weight distribution parameter affecting τ_c is not M_w/M_n but M_z/M_w is due to the following two reasons: first, if M_w/M_n affects τ_c, τ_c of cat.-B PPs must be higher than that of cat.-A PPs at the high molecular weight region because the M_w/M_n of cat.-B PPs is higher than that of cat.-A PPs also at the high molecular weight region, as shown in Figure 3, but the experimental results were not the case. Second, although M_w/M_n is almost constant independent of the molecular weight for cat.-B PPs, M_z/M_w increases with decreasing the molecular weight. From the above, it may be concluded that the critical shear stress of PP scarcely depends on the molecular weight and is higher as the molecular weight distribution M_z/M_w is broader.

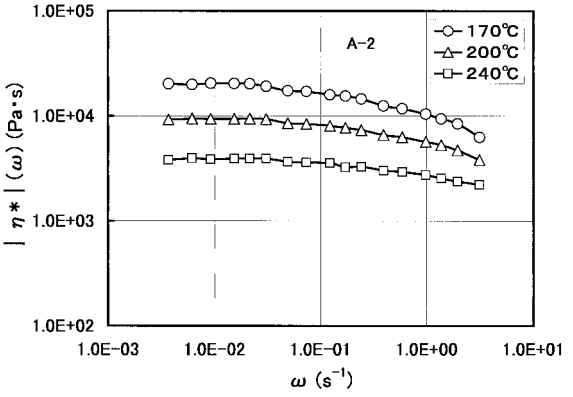

Figure 12 Change of absolute value of complex viscosity $|\eta^*|(\omega)$ with angular frequency ω for A-2 sample.

The following conclusions have been obtained from the above experimental results of melt fracture: the critical shear rate $\dot{\gamma}_c'$ depends on the extrusion temperature, the molecular weight M_w, and the molecular weight distribution M_z/M_w, and increases with increasing the temperature and M_z/M_w^2. The critical shear stress τ_c scarcely depends on the extrusion temperature and molecular weight, and increases with broadening the molecular weight distribution M_z/M_w.

Dynamic Viscoelasticity

Dependence of Complex Viscosity, Zero-Shear Viscosity, and Characteristic Relaxation Time on Temperature and MFI

Figure 12 shows, as an example, the absolute values of complex viscosity $|\eta^*|(\omega)$ of A-2 sample

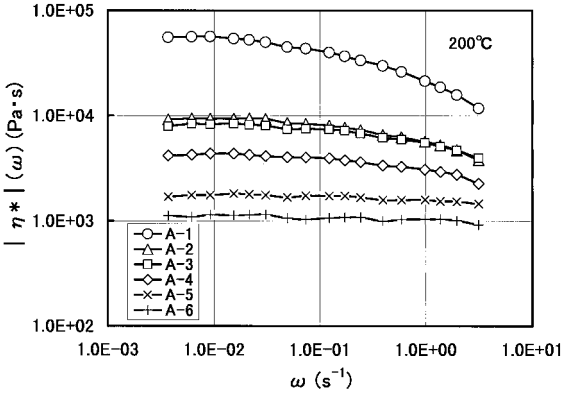

Figure 13 Change of absolute value of complex viscosity $|\eta^*|(\omega)$ with angular frequency ω for cat.-A PPs at 200°C.

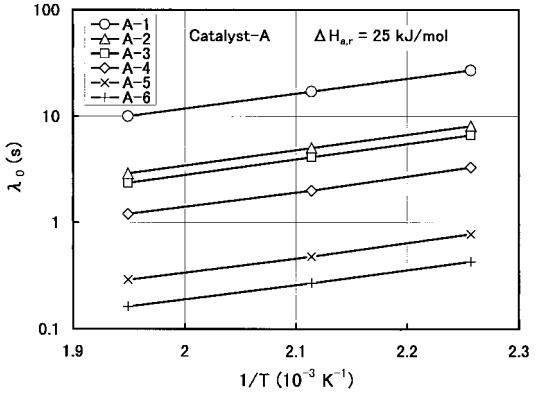

Figure 15 Arrhenius plot of characteristic relaxation time λ_0 for cat.-A PPs.

measured at various temperatures, and Figure 13 shows, as an example, $|\eta^*|(\omega)$s of cat.-A PPs measured at 200°C. Behaviors from Newtonian region to non-Newtonian region are observed. $|\eta^*|(\omega)$ is lower as the temperature and MFI are higher.

Figure 14 shows the Arrhenius plots, according to eq. (9), of the zero-shear viscosity η_0 obtained from eq. (8).

$$\eta_0 = \lim_{\omega \to 0} |\eta^*|(\omega) \tag{8}$$

$$\eta_0 = A \exp \frac{\Delta H_{a,f}}{RT} \tag{9}$$

Similar plots were obtained for cat.-B PPs. The activation energy obtained from the slopes, $\Delta H_{a,f}$ is about 42 kJ/mol, independent of MFI for both PPs. Similar values are reported by other researchers.[19,47–54]

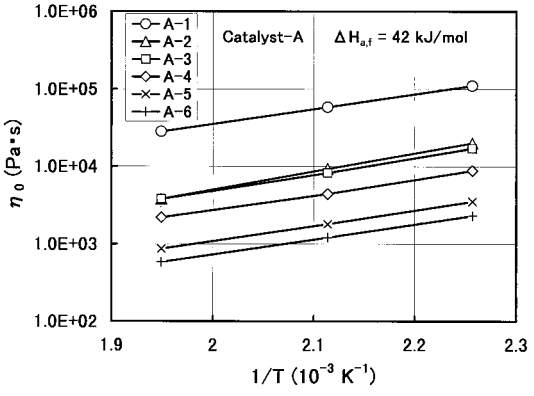

Figure 14 Arrhenius plot of zero-shear viscosity η_0 for cat.-A PPs.

Arrhenius plots of the characteristic relaxation time λ_0 obtained from $|\eta^*|(\omega)$ by use of eq. (7) are shown in Figure 15. Similar plots were obtained for cat.-B PPs. The activation energy of relaxation $\Delta H_{a,r}$ is about 25 kJ/mol, independent of MFI for both series PPs. Dunlop and Williams[50] report the value of $\Delta H_{a,r}$ to be about 42 kJ/mol, which is almost the same as that of $\Delta H_{a,f}$. Ottani et al.[51] report the value of $\Delta H_{a,r}$ to be slightly (about 10%) less than that of $\Delta H_{a,f}$. The $\Delta H_{a,r}$ value of the present study is far less than these previously reported values.

The steady-state compliance J_e^0 can be calculated from the zero-shear viscosity η_0 and characteristic relaxation time λ_0 by the following equation:

$$J_e^0 = \frac{\lambda_0}{\eta_0} \tag{10}$$

Therefore, the activation energy of the steady-state compliance $\Delta H_{a,c}$ is calculated by entering the Arrhenius equations for J_e^0, λ_0, and η_0 into eq.(10), and hence, by eq. (11). Its value is about -17 kJ/mol, which means that J_e^0 $(=\lambda_0/\eta_0)$ increases with increasing temperature.

$$\Delta H_{a,c} = \Delta H_{a,r} - \Delta H_{a,f} \tag{11}$$

$\Delta H_{a,f}$, $\Delta H_{a,r}$, and $\Delta H_{a,c}$ do not have clear physical or chemical meaning. However, they are measures for the degree of temperature changes of η_0, λ_0, and J_e^0.

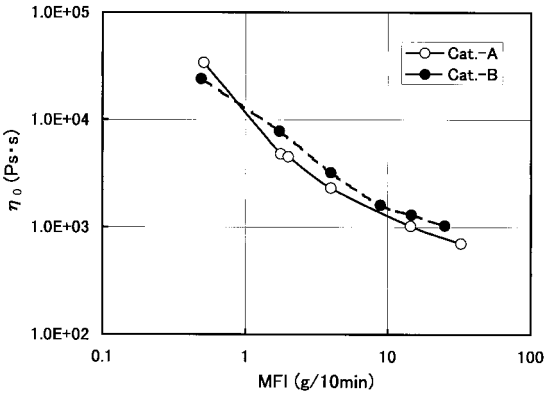

Figure 16 Relation between zero-shear viscosity η_0 and melt flow index (MFI).

In general, beginning with the Rouse theory,[55] many viscoelasticity theories such as the Bueche theory[56] and Doi-Edwards theory[57,58] predict that J_e^0 is proportional to the reciprocal of absolute temperature and slightly decreases with increasing temperature. Namely, $\Delta H_{a,c}$ is a little positive, substantially being 0. Accordingly, the experimental results in the present study are irrational. However, facts seeming such irrational have so far been reported. First as for PP, Ottani et al.[51] showed that $\Delta H_{a,c}$ obtained from λ_0/η_0 shows slightly negative value, as mentioned above. Plazek et al.[59] showed that J_e^0 of a polystyrene (PS) measured by creep experiment decreases with decreasing temperature toward T_g below 40°C. Penwell et al.[60] report that because the temperature dependence of the characteristic relaxation time where a non-Newtonian flow begins is weaker than that of the zero-shear viscosity for a PS melt like the present study, λ_0/η_0 decreases with decreasing temperature at a temperature range of 150–190°C. Heron et al.[61] measured J_e^0 of a PS melt by means of die swell, stress relaxation after cessation of steady-state flow, and first normal stress difference independently, and found that J_e^0 measured by any method increases with increasing temperature in a range of 160–200°C. Han et al.[62] measured the steady-state compliance J_e of an LDPE melt by means of first normal stress difference and found that J_e at low shear rate where J_e approaches the zero-shear steady-state compliance J_e^0 increases with increasing temperature. Sakai et al.[63] measured J_e^0 of a pitch from shear creep experiment and found that it is proportional to temperature. As mentioned above, because other researchers also report irrational phenomena at a look that J_e^0 increases with increasing temperature, which is similar to the experimental results of the present study, some substantial fact that cannot be explained by the common sense may be hidden.

Figure 16 shows the relation between the zero-shear viscosity η_0 and MFI. There exist relations with slopes of about -1 in the log–log plot of the two quantities. cat.-A PPs show higher η_0 than cat.-B PPs at low MFI region and cat.-A PPs show inversely lower η_0 than cat.-B PPs at MFI > 0.8 g/10min. Because η_0 is the viscosity at shear rate or shear stress of 0 and MFI is a quantity proportional to the reciprocal of viscosity at a shear stress of 2×10^4 Pa, there exists a relation of nearly inverse proportionality between the two, this relation being delicately different between the two series of PPs in the present study. It is assumed from Figures 12 and 13 that a non-Newtonianity already manifests at the shear stress of MFI measurement, and the molecular weight distribution characteristics of the two series of PPs affect the relationship.

Figure 17 shows the relation between the characteristic relaxation time λ_0 and MFI. Although the log–log plot of λ_0 against MFI shows a linear relationship with a slope of -1 for cat.-A PPs, the slope of the plot decreases with increasing MFI for cat.-B PPs. Furthermore, cat.-B PPs show shorter λ_0 than cat.-A PPs at the low MFI region, and cat.-B PPs show inversely longer λ_0 than cat.-A PPs at MFI > 2 g/10 min. This feature is very similar to the change of M_z/M_w with MFI in Figure 3, and it is assumed that the molecular weight distribution parameter M_z/M_w affects λ_0. This will be referred to again later in relation with Figure 22. Mieras et al.[5] showed a linear

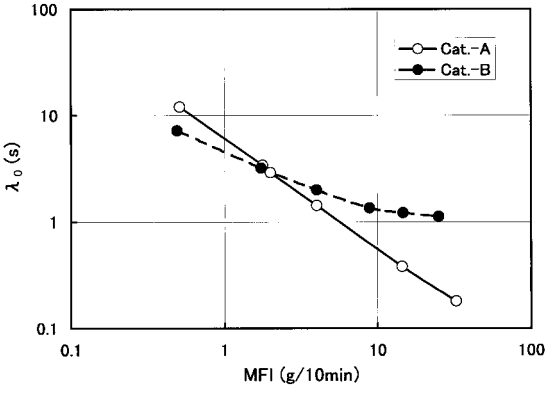

Figure 17 Relation between characteristic relaxation time λ_0 and melt flow index (MFI).

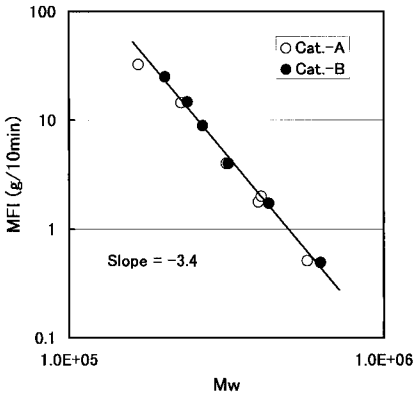

Figure 18 Relation between melt flow index (MFI) and weight-average molecular weight M_w.

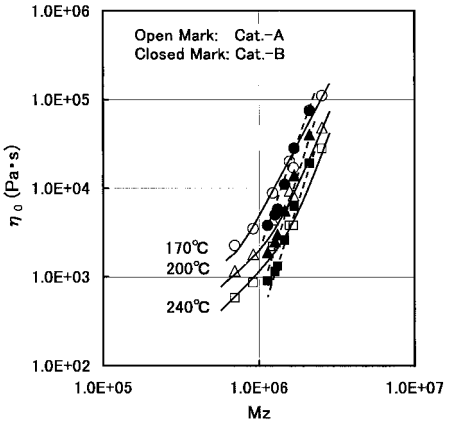

Figure 20 Relation between zero-shear viscosity η_0 and z-average molecular weight Mz.

relationship with a negative slope in the log–log plot of the characteristic relaxation time against MFI, although with large scattering.

Molecular Weight Dependence of Zero-Shear Viscosity and Characteristic Relaxation Time

Figure 18 shows the relation between MFI and weight-average molecular weight M_w. It shows a linear relationship with a slope of -3.4 in a log–log plot, independent of the catalyst system, and the well-known 3.4th-power law[64] holds. Grant and Dieckmann[18] and Bernreitner et al.[65] both report the slope value of -2.9 for various PPs. Tzoganakis et al.[21] report a value of -3.3 for controlled rheology PPs.

Figure 19 shows the relation between zero-shear viscosity η_0 and weight-average molecular weight M_w. The relation is not linear[64] but curved downward in a log–log plot, and the slope is slightly steeper for cat.-A PPs than for cat.-B PPs. However, the difference is small. Figure 20 shows the relation between η_0 and z-average molecular weight M_z. Here, contrary to the case of the M_w in Figure 19, the slope of the relation curve is steeper for cat.-B PPs than for cat.-A PPs, the difference being larger than that in the case of M_w. From the above, it may be said that η_0 is governed by an average molecular weight of slightly higher order than the weight-average molecular weight M_w. This agrees with the prediction of the Bueche theory.[66] He showed theoretically that the average molecular weight that determines η_0 is one between M_w and M_z.

Figures 21 and 22 show the relations between the characteristic relaxation time λ_0 and M_w and M_z, respectively. The relation between λ_0 and M_z is linear, with a slope of about 3.3 in a log–log plot, independent of the catalyst system. From

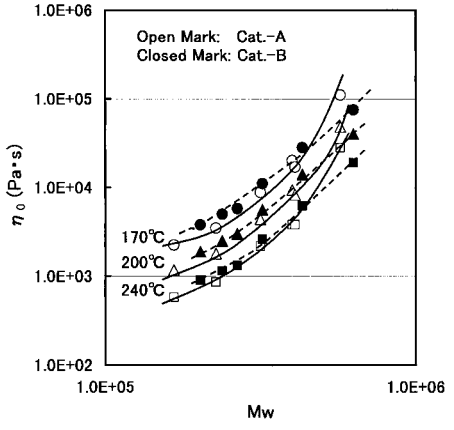

Figure 19 Relation between zero-shear viscosity η_0 and weight-average molecular weight M_w.

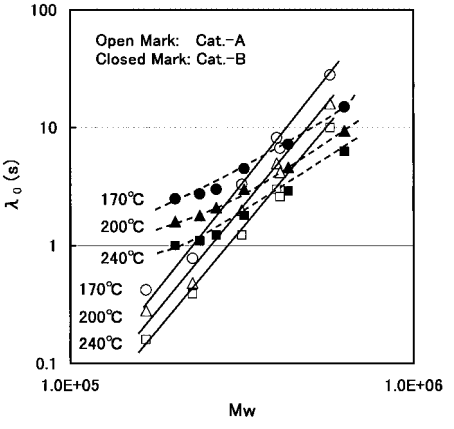

Figure 21 Relation between characteristic relaxation time λ_0 and weight-average molecular weight M_w.

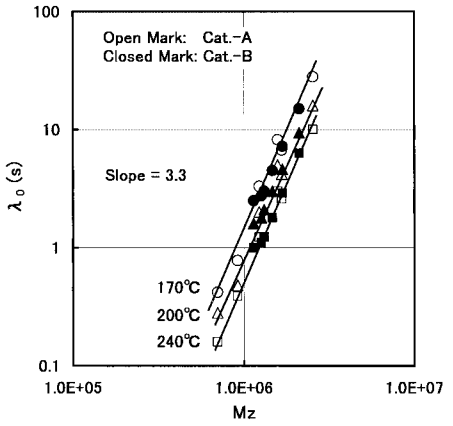

Figure 22 Relation between characteristic relaxation time λ_0 and z-average molecular weight M_z.

this, it may be said that λ_0 is determined by M_z. Ottani et al.[51] obtained the characteristic relaxation time λ_0 from the absolute value of complex viscosity for usual PPs and controlled rheology PPs by the same manner as the present study and plotted log λ_0 against log M_w. As a result, two series PPs show different linear relations. However, the present authors plotted log λ_0 against log M_z using their data shown in their article,[51] and obtained a linear relation with a slope of 2.7, independent of the series of PPs. This supports the conclusion of the present study. Bernreitner et al.[65] showed that the log–log plot of λ_0 against M_w of various types of PPs is linear though with large scattering. To our regret, because they do not show the value of M_z, we could not study the plot of λ_0 against M_z.

Relation between Storage Modulus and Loss Modulus

Chuang and Han[67] first used the log–log plot of the storage modulus G' against the loss modulus G'' to put in order the dynamic viscoelasticities of polymer blends. Harrell and Nakajima[68] used the same plot to explain the effect of long chain branching on the rheological properties of ethylene–propylene copolymers. Following them, many researchers have used the plot mainly in studying the viscoelasticities of polymer blends. As a result, it has been found that a log G'–log G'' plot, like the log–log plot of the first normal stress difference against shear stress, is expressed by a curve akin to a straight line, substantially independent of temperature for homopolymers and compatible polymer blends. Also found is that such a plot is sensitive to the morphological state for incompatible polymer blends. Furthermore, it is suggested that such a plot can be used to evaluate the relative intensity of elasticity to viscosity of a system. As for the effect of molecular weight distribution, the following studies are reported: Harrell and Nakajima[68] introduced long chain branchings to an ethylene–propylene copolymer by adding to it various amounts of dicumyl peroxide and then melt-mixing, and measured their melt dynamic viscoelasticities. They found that G' at a constant G'' is the higher for the sample prepared with a larger content of peroxide and, hence, with broader molecular weight distribution as well as with more long chain branchings. Han[69] showed experimentally and theoretically by use of a blend theory that, for the binary blends of the same kind of polymers, G' at a constant G'' of the blends are higher than those of the components. Han and Kim[70] applied the tube model theory[57] to the mixtures of compatible polymer blends and calculated their linear viscoelastic properties. As a result, they showed that the log G'–log G'' line shifts to a higher G' side as well as its slope decreasing from two of the monodis-

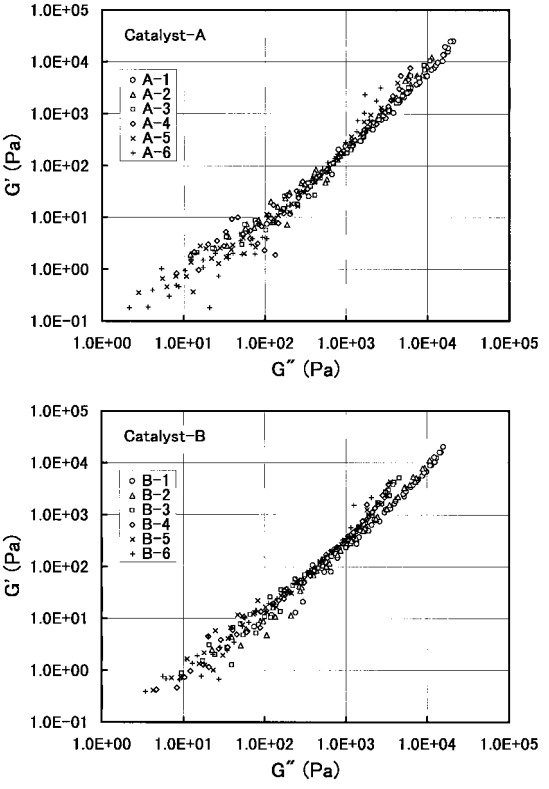

Figure 23 (a) Plots of storage modulus G' against loss modulus G'' for cat.-A PPs. (b) Plots of storage modulus G' against loss modulus G'' for cat.-B PPs.

perse polymers with broadening the molecular weight distribution for the binary mixtures of the same kind of polymers as a special case.

Figure 23(a) and (b) shows log G'–log G'' plots measured at various temperatures for cat.-A PPs and cat.-B PPs, respectively. Although data points scatter particularly at low and high modulus regions due to the low measurement precision of G' for both series PPs, they are on a curve akin to a straight line with a slope of 1.2–1.3, independent of MFI and temperature. Comparing at the same G'', cat.-A PPs show slightly lower G' than cat.-B PPs, which means that the elasticity of cat.-A PPs is weaker than that of cat.-B PPs. This corresponds to the fact that the end correction coefficient ν (Fig. 6) and the die swell ratio D/D_0 (Fig. 7) in capillary flow properties are lower for cat.-A PPs than for cat.-B PPs, and assumed, by reference to the above-mentioned previous studies, that this is because cat.-A PPs show narrower molecular weight distribution (M_w/M_n) than cat.-B PPs. Although little difference is observed between the slopes of log G'–log G'' plots of both series PPs, they are considerably easier than two of the theoretical value for monodisperse polymer.

CONCLUSIONS

The molecular weight distribution characteristics and the rheological characteristics are compared between two series of PPs prepared by the $MgCl_2$-supported titanium catalyst (cat.-A PPs) and by the $TiCl_3$-type catalyst (cat.-B PPs), and the relations between the two characteristics are investigated.

1. The shape of molecular weight distribution of cat.-A PPs scarcely depends on MFI and the curve shifts in parallel to the molecular weight axis according to MFI. On the other hand, for cat.-B PPs, not only the curve shifts but also the shape at the high molecular weight side narrows with decreasing the MFI.
2. M_w/M_n, a measure of molecular weight distribution, scarcely depends on MFI for both series PPs, and their values are 5.5 and 9 for cat.-A PPs and cat.-B PPs, respectively. M_z/M_w, a parameter of molecular weight distribution at the high molecular weight region, increases with increasing MFI for cat.-B PPs, whereas it scarcely depends on MFI for cat.-A PPs. As a result, cat.-A PPs show higher M_z/M_w than cat.-B PPs at MFI $<$ 2 g/10 min, and cat.-B PPs show higher M_z/M_w at higher MFI.
3. Little substantial difference is observed between both series PPs in the flow curve at high shear rates that a polymer melt encounters at extrusion and injection molding.
4. The end correction coefficient and die swell ratio, which are measures of melt elasticity, is lower for cat.-A PPs than for cat.-B PPs.
5. cat.-A PPs show higher critical shear rates at which a melt fracture begins to occurs than cat.-B PPs at low MFI, and cat.-B PPs inversely show higher critical shear rates than cat.-A PPs at high MFI. Although the critical shear stress of cat.-A PPs is almost constant, independent of MFI, that of cat.-B PPs tends to increase with increasing MFI. These originate from the different changes of M_z/M_w with MFI for both series PPs.
6. The zero-shear viscosity and characteristic relaxation time, particularly the latter, are higher for cat.-A PPs at the low MFI region and for cat.-B PPs at the high MFI region. This also originates from the different changes of M_z/M_w with MFI.
7. Compared at the same loss modulus, cat.-A PPs show slightly lower storage modulus than cat.-B PPs, which means that the elasticity of cat.-A PPs is weaker than that of cat.-B PPs. This originates from narrower molecular weight distribution (M_w/M_n) of the former.

The authors would like to thank Tokuyama Corp. for permission to publish this article.

REFERENCES

1. Bagley, E. B. J Appl Phys 1957, 28, 624.
2. Rabinowitsch, B. Z. Z Physik Chem (Leipzig) 1929, A145, 1.
3. Graessley, W. W. Adv Polym Sci 1974, 16, 1.
4. Frank,Von H. P. Rheol Acta 1966, 5, 89.
5. Mieras, H. J. M. A.; Van Rijn, C. F. H. J Appl Polym Sci 1969, 13, 309.
6. Yamauchi, S.; Yasuno, K. Kogyo Kagaku Zasshi 1963, 66, 1468.
7. Kamide, K.; Fujii, K. Kobunshi Kagaku 1967, 24, 120.

8. Arai, T.; Aoyama, H.; Suzuki, I. Kogyo Kagaku Zasshi 1960, 63, 418.
9. Fukazawa, Y. Kogyo Kagaku Zasshi 1960, 63, 459.
10. Ryder, L. B. SPE J Dec. 1961, 1305.
11. Shott, H. J. J Polym Sci Part A 1964, 2, 3791.
12. Ram, A.; Narkis, M. J Appl Polym Sci 1966, 10, 361.
13. Fujiki, T.; Uemura, M.; Kosaka, Y. J Appl Polym Sci 1968, 12, 267.
14. Kataoka, T.; Ueda, S. J Appl Polym Sci 1968, 12, 939.
15. Fujiyama, M.; Ohba, S.; Awaya, H. Kobunshi Ronbunshu 1975, 32, 418.
16. LaMantia, F. P.; Valenza, A.; Acierno, D. Rehol Acta 1983, 22, 299.
17. Fujiyama, M.; Wakino, T. Nihon Reoroji Gakkaishi 1991, 19, 64.
18. Grant, D. E.; Dieckmann, S. F. J Appl Polym Sci 1965, 9, 3231.
19. Fujiyama, M.; Awaya, H. J Appl Polym Sci 1972, 16, 275.
20. Fujiyama, M.; Kagiyama, Y. Kobunshi Kagaku 1972, 29, 191.
21. Tzoganakis, C.; Vlachopoulos, J.; Hamielec, A. E. Polym Eng Sci 1989, 29, 390.
22. Arai, T.; Aoyama, H. Trans Soc Rheol 1963, 7, 333.
23. Kawasaki, N.; Ohno, S.; Fukuda, M. Kobunshi Kagaku 1973, 30, 485.
24. Kawasaki, N.; Ohno, S. Kobunshi Ronbunshu 1974, 31, 1.
25. Kamide, K.; Inamoto, Y.; Ohno, K. Kobunshi Kagaku 1965, 22, 529.
26. Beynon, D. L. T.; Glyde, B. S. Br Plast 1960, 33, 414.
27. Rogers, M. G. J Appl Polym Sci 1970, 14, 1679.
28. Fleissner, Von M. Angew Makromol Chem 1973, 33, 75.
29. Kawasaki, N.; Yamagata, Y.; Ohno, S.; Hahsimoto, T. Nihon Gomu Kyokaishi 1973, 16, 502.
30. Spencer, R. S.; Dillon, R. E. J Colloid Sci 1949, 4, 241.
31. Mills, D. R.; Moore, G. E.; Pugh, D. W. SPE Trans 1961, 1, 40.
32. Bagley, E. B. Trans Soc Rheol 1961, 5, 355.
33. Doring, G.; Leusering, H. J. Kunststoffe 1963, 53, 11.
34. Sieglaff, C. L. SPE Trans 1964, 4, 459.
35. Stabler, H. G.; Haward, R. N.; Wright, B. Adv Polym Sci Technol S. C. I. Monogr No.6 1967, 327.
36. Goyal, S. K.; Kazatchkov, I. B.; Bohnet, N.; Hatzikiriakos, S. G. SPE Technical Paper 55th ANTEC 1997, 43, 1076.
37. Dennison, M. T. Trans J Plast Inst 1967, 35, 803.
38. Bartoš, O. J Appl Phys 1964, 35, 2767.
39. Vinogradov, G. V.,; Malkin, A. Ya.; Leonov, A. I. Kolloid-Z Z Polym 1963, 191, 25.
40. Vinogradov, G. V.; Friedman, M. L.; Yarlykov, B. V.; Malkin, A. Ya. Rheol Acta 1970, 9, 323.
41. Baik, J. J.; Tzoganakis, C. Polym Eng Sci 1998, 38, 274.
42. Howells, E. R.; Benbow, J. J. Trans J Plast Inst 1962, 30, 240.
43. Vlachopoulos, J.; Lidorikis, S. Polym Eng Sci 1971, 11, 1.
44. Paradis, R. A. SPE J 1967, 23, 54.
45. Vlachopoulos, J.; Alam, M. Polym Eng Sci 1972, 12, 184.
46. Ferguson, J.; Wright, B.; Haward, R. N. J Appl Chem 1964, 14, 53.
47. Graessley, W. W.; Segal, L. Macromolecules 1969, 2, 49.
48. Vinogradov, G. V.; Prozorovskaya, N. V. Rheol Acta 1964, 3, 156.
49. van der Vegt, A. K. Trans J Plast Inst 1964, 32, 165.
50. Dunlop, A. N.; Williams, H. L. J Appl Polym Sci 1970, 14, 2753.
51. Ottani, S.; Pezzin, P.; Castellari, C. Rheol Acta 1988, 27, 137.
52. Pearson, D. S.; Fetters, L. J.; Younghouse, L. B.; Mays, J. W. Macromolecules 1988, 21, 478.
53. Fujiyama, M.; Kawamura, Y.; Asaeda, E. Nihon Reoroji Gakkaishi 1989, 17, 48.
54. Eckstein, A.; Friedrich, C.; Lobbrecht, A.; Spitz, R.; Mülhaupt, R. Acta Polym 1997, 48, 41.
55. Rouse, P. E., Jr. J Chem Phys 1953, 21, 1272.
56. Bueche, F. J Chem Phys 1954, 22, 603.
57. Doi, M.; Edwards, S. F. J Chem Soc Faraday Trans 2 1978, 74, 1789, 1802, 1818.
58. Graessley, W. W. J Polym Sci Polym Phys Ed 1980, 18, 27.
59. Plazek, D. J.; O'Rourke, V. M. J Polym Sci A-2 1971, 9, 209.
60. Penwell, R. C.; Graessley, W. W. J Polym Sci Polym Phys Ed 1974, 12, 1771.
61. Heron, H. S.; Pederson, S.; Chapoy, L. L. Rheol Acta 1976, 15, 379.
62. Han, C. D.; Lem, K. W. Polym Eng Rev 1982, 2, 135.
63. Sakai, M.; Inagaki, M. Nihon Reoroji Gakkaishi 1987, 15, 76.
64. Bueche, F. J Chem Phys 1956, 25, 599.
65. Bernreitner, K.; Niessl, W.; Gahleitner, M. Polym Test 1992, 11, 599.
66. Bueche, F. J Polym Sci 1960, 43, 527.
67. Chuang, H. K.; Han, C. D. J Appl Polym Sci 1984, 29, 2205.
68. Harrell, E. R.; Nakajima, N. J Appl Polym Sci 1984, 29, 995.
69. Han, C. D. J Appl Polym Sci 1988, 35, 167.
70. Han, C. D.; Kim, J. K. Macromolecules 1989, 22, 1914, 4292.